Pergamon

Cement and Concrete Research 30 (2000) 403–410

CEMENT AND CONCRETE RESEARCH

Polyolefin fiber-reinforced concrete composites Part II. Damping and interface debonding☆

L. Yan[a], C.H. Jenkins[b,*], R.L. Pendleton[b]

[a]*Pro-Eco, Oakville, Ontario, L6H 5V9, Canada*
[b]*Department of Mechanical Engineering, South Dakota School of Mines and Technology, Rapid City, SD 57701, USA*

Received 2 November 1998; accepted 13 December 1999

Abstract

Two damping mechanisms are suggested to explain the high damping found from preliminary dynamic testing of polyolefin fiber-reinforced concrete composites (FRC). A significant interfacial relative displacement, which may cause debonding and corresponding interfacial friction, is suggested as the fundamental energy dissipation mode during vibration. Such a displacement may easily take place over a great fraction of an interface between low-aspect ratio fiber and cementitious matrix, resulting in high damping in crimped FRC. Debonding at the intersections of microcracks in matrix and fiber due to the crack opening under tensile strain also consumes vibration energy, producing extra damping in fine FRC. In order to gain high damping without seriously degrading other mechanical properties of FRC, a combination of reinforcing fibers with different geometric features is suggested.

Keywords: Composite; Polyolefin fiber

1. Introduction

Recent research [1–3] on dynamic properties of polyolefin fiber-reinforced concrete composites (FRC) has shown that fibers with a crimped surface or wavy geometry (crimped fiber), and with a smooth surface but small diameter (fine fiber of 6 mils in diameter), produced a significant increase in damping and a discernible decrease in response frequency. Another dynamic characteristic found in these damping-improved composites is that the damping ratio in the first vibration cycle, ζ_1, is much greater than that in the following cycles (say ζ_{10}), as shown in Fig. 1. The reader may refer to Refs. [1–3] for the experimental details including fibers and compositions of the FRC used in the study.

These phenomena cannot be explained by the rule of mixtures, viscoelastic or hysteretic damping in the matrix due to the stress concentration in the vicinity of fiber–matrix interface or cracking of the cementitious matrix [1,2].

Recent works [1,4] on direct observation of the interfaces between polyolefin fiber and cementitious matrix under a scanning electron microscope (SEM) show that the bond between fiber and concrete is mainly mechanical. The interface bond may be strengthened by interfacial roughness and anchoring of fiber tendrils in the matrix, which results as a by-product of mixing of fibers in cementitious mix. If there is no such interfacial asperity, the bond strength will be merely static friction, mainly depending on the normal pressure, which the matrix exerts on the fiber surface. Thus, the bond strength would not be expected to be very strong. A debonding (breaking a compact interface), followed by an interfacial slip, will take place when the shear stress on the interface is greater than the bond strength or, alternatively, an interfacial relative displacement is greater than a critical value that the interfacial bond can bear. This debonding is, indeed, an interfacial fracture [5], which starts at bond strength and ends at a frictional shear stress. This is also a necessary stage preceding the interfacial slip, which is a relative movement between fiber and matrix along the interface. The debonding may take place at the ends of an interface and at the intersections of a crack and fiber, where the shear strain may be great enough to break bonds. The relative importance of these mechanisms depends on the magnitude of the interfacial relative displacement.

☆ This paper was originally submitted to Advanced Cement Based Materials. The paper was received at the Editorial Office of Cement and Concrete Research on 2 November 1998 and accepted in final form on 13 December 1999.

* Corresponding author. Tel.: +1-605-394-2406; fax: +1-605-394-2405.
E-mail address: cjenkins@taz.sdsmt.edu (C.H. Jenkins).

0008-8846/00/$ – see front matter
PII: S0008-8846(99)00268-9

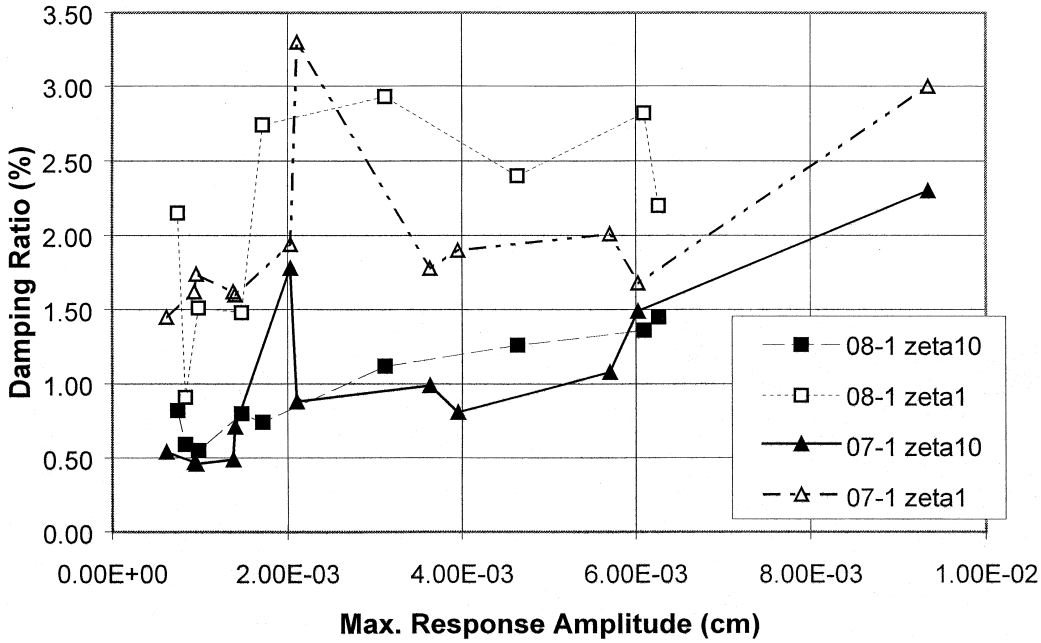

Fig. 1. A comparison of damping ratio between ζ_1 and ζ_{10} under various maximum response amplitudes in a crimped fiber-reinforced concrete composite, FRC07-1, and a fine fiber-reinforced one, FRC08-1, noting that ζ_1 was about a double ζ_{10}.

In this paper, we present the damping mechanisms in FRC, which are directly related to interfacial debonding and friction resulting from the interfacial relative displacement. The interfacial relative displacement is analyzed based on strains along an interface with various fiber aspect ratios. Energy dissipated due to crack opening is calculated and compared with experimental results. It is intended to provide preliminary understanding for further investigation and design of FRC with good damping properties.

2. Strain distributions in a beam subject to flexural vibration

A beam in a free transverse, or flexural, vibration is subjected to flexural deformation according to its fundamental modes. The strain in the beam along the beam neutral axis direction, x, can be calculated once the deflection or mode shape, $v(x)$, is known [6]. The relation between the strain, ε, in a beam fiber and the curvature of the deflection (which is proportional to second derivative of deflection for small deflection), is expressed as [7]

$$\varepsilon = y\frac{\mathrm{d}^2 v}{\mathrm{d}x^2} \tag{1}$$

where y is the distance from a beam fiber to the neutral axis of the beam. For generality, the normalized first mode shape $v(x/l)$ [8] of a free-free beam with unit length, and the corresponding curvature along the beam axis are illustrated in Fig. 2. The normalized distribution of axial strain, depending on the distance from the neutral axis, should be similar to the curvature because there exists the proportion-

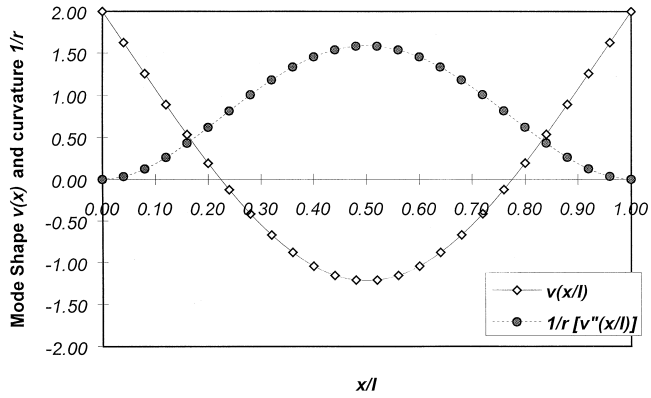

Fig. 2. The first normalized mode shape and curvature distributions in a free-free beam.

ality between strain and the curvature, as indicated by Eq. (1). Fig. 2 implies that the maximum strain in a free-free beam always takes place in the outermost beam fiber (axially) located in the middle (longitudinally) of the beam, where the displacement is not necessarily the maximum. At the ends of the beam, however, there is no strain although maximum displacement occurs there.

A strain distribution for a beam of length l can be derived from the normalized mode shape $v(x/l)$. Assuming the maximum vibration amplitude measured at one end of the beam is A_M (hereafter, the subscript capital M denotes "maximum"), it can be shown as [1]

$$\varepsilon = \frac{A_M y}{2l^2}\left[\frac{d^2 v(x/l)}{dx^2}\right]. \quad (2)$$

Given l=30 cm (12 in.) for the specimens used and A_M measured at either end of a beam, the maximum (axial) strains in the middle of the beam, where y=1.25 cm (0.5 in.), for example, are $\varepsilon_M = 1.1 \times 10^{-6}$ for an A_M=0.001 cm, and $\varepsilon_M = 8.8 \times 10^{-6}$ for A_M=0.008 cm. The order of these strains seems very reasonable compared to the failure strain of concrete [9], which is around 50×10^{-6} in tension.

3. Stress and relative displacement distributions along fiber–matrix interface

A cylindrical matrix with a fiber embedded at its center is selected as a representative volume element (RVE) that is located in the surface layer in the middle of a free-free beam, as shown in Fig. 3. The fiber is assumed to be parallel to the neutral axis of the beam, and therefore, the stress or strain in tension or in compression caused by vibration deflection is parallel to the fiber–matrix interface. The diameter of the RVE is determined according to the fiber volume fraction, i.e., the specimen is assumed to be a compact stack of such RVEs. In this case, it can be shown that the ratio of RVE diameter to the fiber diameter is approximately the reciprocal of the square root of the fiber volume fraction [10]. It should be noted that the fibers in the beam specimen were, in fact, randomly oriented. With the above assumption, however, the analysis of stress and relative displacement along an interface is simplified.

As the beam is deflected due to a flexural vibration, the surfaces of the fiber and the matrix along the interface may be both stretched or compressed before an interfacial debonding takes place. A relative displacement occurs between fiber and matrix because of the difference between the stretches caused by the necessity of force transfer across the interface through shear. According to Cox's assumption [11] and Kelly's extension [12], the interface shear stress is proportional to the difference between u and w, where u is the axial displacement at a point in the fiber and w is the axial displacement the matrix would have at the same point in the matrix with no fiber present. The rate of change of the axial force P in fiber is given by [13]

$$\frac{dP}{dx} = k_{int}(u - w) \quad (3)$$

where k_{int} is a proportionality constant to be determined from geometrical and material property data, i.e.,

$$k_{int} = \beta^2 A_f E_f \quad (4)$$

and

$$\beta^2 = \frac{2\pi G_M}{A_f E_f \ln(D/d_f)} \quad (5)$$

where A_f is the cross-section area of the fiber, E_f is the elastic modulus in the fiber axial direction, G_m is the shear modulus of the matrix, D is the diameter of the effective matrix cylinder, D_f is the fiber diameter, and the diameter

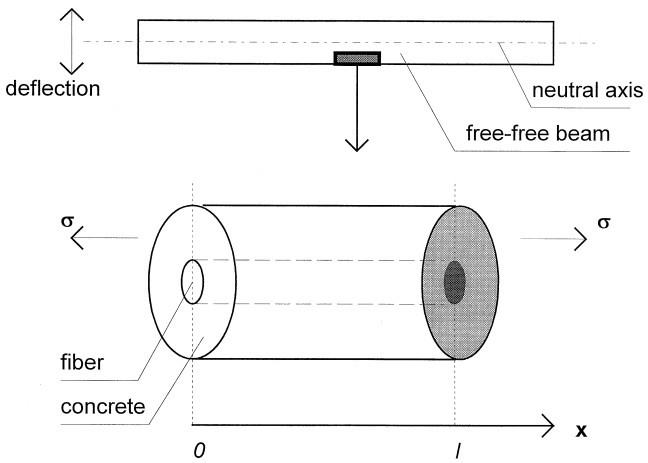

Fig. 3. Schematic of one-fiber-matrix cylinder (RVE) taken from the surface layer located in the middle of a free-free beam, where the strain in matrix is maximum.

ratio, D/d_f, is [10]

$$\frac{D}{d_f} = \frac{0.952}{V_f^{1/2}} \tag{6}$$

and V_f is the fiber volume fraction in Eq. (6).

The stress in the fiber and shear stress along the interface are, therefore, given by [13]

$$\sigma_f = \frac{P}{A_f} = E_f \varepsilon_m \left[1 - \frac{\cosh[\beta(05l - x)]}{\cosh(0.5\beta l)}\right] \tag{7}$$

$$\tau = \frac{d_f E_f \varepsilon_m \beta}{4} \left[\frac{\sinh[\beta(0.5l - x)]}{\cosh(0.5\beta l)}\right] \tag{8}$$

where ε_m is the axial strain in the matrix.

The relative displacement can be derived by rearranging Eq. (3) and is

$$u - w = \frac{1}{k_{int}} \frac{dP}{dx}. \tag{9}$$

Substituting P from Eq. (7) into Eq. (9), and noting Eq. (4), yields

$$u - w = \frac{\varepsilon_m}{\beta} \left[\frac{\sinh[\beta(0.5l - x)]}{\cosh(0.5\beta l)}\right]. \tag{10}$$

Eqs. (8) and (10) show that the variations of interfacial shear stress and relative displacement have the same trend along the fiber axis. Letting the fiber be of a circular cross-section, substituting d_f into Eq. (5), yields Eq. (11)

$$\beta = \frac{1}{d_f} \sqrt{\frac{8G_m}{E_f \ln(D/d_f)}}. \tag{11}$$

Assuming $V_f = 0.01$, using $G_m = 11.7$ GPa for matrix and $E_f = 8.0$ GPa [9] for a drawn fiber, we have

$$\beta = \frac{2.28}{d_f}. \tag{12}$$

In order to show the effect of fiber aspect ratio, i.e., length to diameter (l/d_f), on a relative displacement, we can rearrange the variable term in Eq. (10) by noting Eq. (12) as Eq. (13)

$$\beta(0.5l - x) = 2.28 \frac{l}{d_f} \left(0.5 - \frac{x}{l}\right). \tag{13}$$

Now, Eq. (10) becomes

$$u - w = \frac{\varepsilon_m}{\beta} \left\{\frac{1}{\cosh(0.5\beta l)} \sinh\left[2.28 \frac{l}{d_f} \left(0.5 - \frac{x}{l}\right)\right]\right\}. \tag{14}$$

Variations of the normalized relative displacement, calculated from the terms in the curly brackets of Eq. (14), along the fiber axial direction for different fiber aspect ratios, are illustrated in Fig. 4.

It is clear from Fig. 4 that the fraction of an interface which could be subject to a noticeable relative displacement is dependent on the fiber aspect ratio; the smaller the ratio, the greater the fraction. For a fiber with an aspect ratio greater than 85, a minor fraction at the ends of the interface could have a noticeable relative displacement. For a fiber with an aspect ratio less than 10, however, a large fraction of the interface could undergo a certain relative displacement. Fig. 4 also shows that the largest displacements take place at the ends of fibers. Significant relative displacements, therefore, could happen at fiber ends, even though the fiber aspect ratio is great. In any case, at the same fiber volume fraction, the fraction of a total interfacial length that may undergo a significant relative displacement, possibly causing debonding, in a low-aspect ratio fiber-reinforced concrete, is greater than that in a high-aspect ratio fiber-reinforced concrete.

The magnitude of relative displacement and shear stress occurring along an interface is dependent not only on the fiber aspect ratio just discussed, but also on the terms $d_f E_f \varepsilon_m \beta/4$ for stress and on ε_m/β for relative displacement in Eqs. (8) and (10), respectively, where strain in the matrix is a variable. By using Eq. (12), we have

$$\frac{\varepsilon_m}{\beta} = \frac{\varepsilon_m d_f}{2.28} \tag{15}$$

$$\frac{d_f E_f \varepsilon_m \beta}{4} = \frac{2.28 E_f \varepsilon_m}{4}. \tag{16}$$

Eq. (15) indicates that the maximum relative displacement given in Eq. (10) is proportional to the product of the strain in matrix and the diameter of a fiber, implying that a coarse fiber may produce a larger relative displacement than a fine one at the same aspect ratio. Eq. (16) shows that the maximum shear stress given in Eq. (8) is dependent on the modulus of fiber and strain in matrix, and is independent of the diameter of the fiber. When ε_m varies from 1.1×10^{-6} to 8.8×10^{-6} as in our experiments [1,2], the maximum relative displacements at the ends of fibers, ε_m/β, are $(0.73–5.87) \times 10^{-10}$ m for 6-mil fibers and $(3.3–25.5) \times 10^{-10}$ m for 25-mil fibers. If we assume that high damping results from interfacial debonding, the interface shear strength, which is the shear stress at debonding, can be calculated by using Eq. (16) when the strain and the fiber modulus are known. Using experimental data for fine FRC which started a high damping at a strain of 1.1×10^{-6} [1,2] and a modulus of 8.0 GPa [9], the interfacial shear strength is 0.5×10^{-2} MPa. This shear strength seems quite reasonable, though still small, when compared to 1.6×10^{-1} MPa for nylon and $(1.1–2.9) \times 10^{-1}$ MPa for polyester reported by Wang et al. [14].

It should be noted that a certain relative displacement or shear stress does not necessarily mean that there is a debonding or an interfacial slip. Debonding can only take place when the relative displacement or shear stress reaches a critical value, which may correspond to a critical vibration amplitude, and therefore, a critical strain in the matrix.

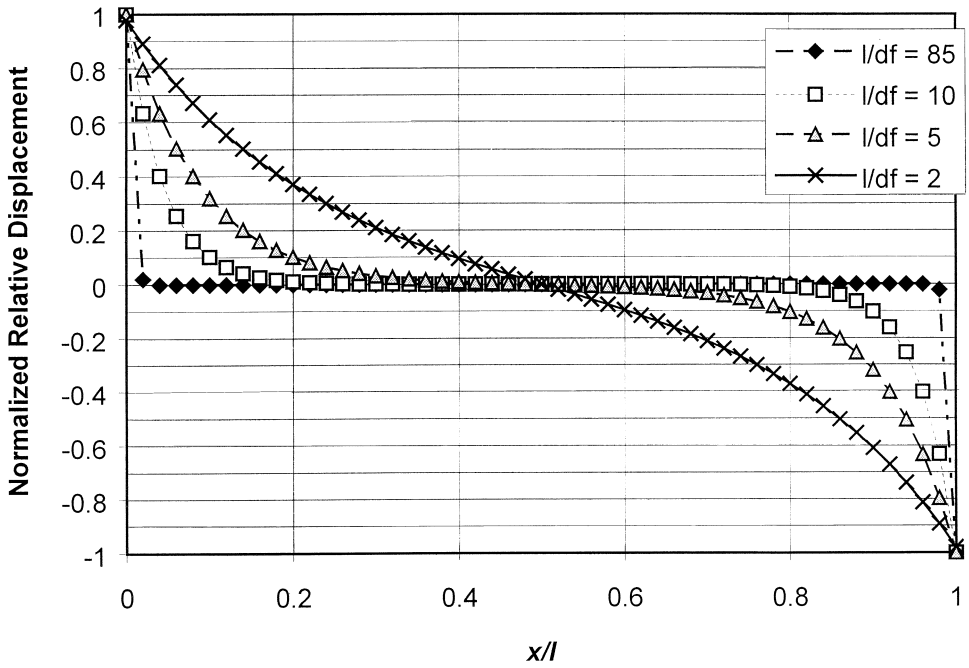

Fig. 4. Variation of normalized relative displacement along interfaces of various aspect ratios.

Above this critical vibration amplitude, a relative displacement could break the interfacial bond. The critical strain corresponding to this critical amplitude can be computed by using Eq. (2) with an experimental amplitude which was around 0.001 cm, noting that only the outermost beam fiber located in the middle of the beam reaches this critical strain at this time. When the amplitude increases above its critical amplitude, a greater portion of the beam (by extending from the middle towards both ends of the beam) reaches and exceeds the critical strain, and therefore, more of the interface may break the interfacial bond. The shear strength also increases since the radial compressive stress across the interface increases with the longitudinal tensile strain in the matrix, due to the transverse contraction of the matrix on the fiber. This leads to dissipating more energy on the interface when interfacial debonding and slip have to take place.

4. Damping mechanism in crimped FRC

As discussed in the previous section, only those fibers with low-aspect ratios may have noticeable debonding, and thus, subsequent interfacial slip in FRCs. Although the

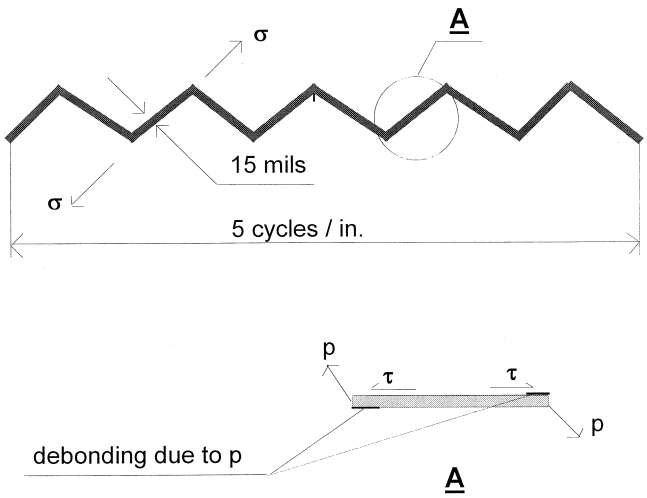

Fig. 5. Schematic of a crimped fiber and its pitch segment acting as a low-aspect ratio fiber, noting that forces from adjacent segments may facilitate debonding at the ends ("A" signifies a magnified view).

fibers used in this study were apparently not low-aspect ratio according to their nominal lengths, the crimped fibers appear to act as fibers of low-aspect ratio. Two kinds of crimped fibers were used in this study, 25 × 2 with a wavy pitch of 4 cycles/in., and 15 × 1 with a pitch of 5 cycles/in., as schematically shown in Fig. 5. Due to crimping, two segments of low-aspect ratio may be assumed in each pitch. The aspect ratios of these segments are of 5 to 10 if fiber diameters and pitches are noticed [1,2]. The direction of stress in the surrounding matrix is not necessarily parallel to the fiber axis but may be parallel to its segment axis. The segment therefore can be considered as an individual low-aspect ratio fiber with extra forces, p, acting at its ends, at an angle with the segment axis (Fig. 5). The extra forces in such directions may facilitate the debonding, in addition to the relative displacements at the fiber ends, thus making the frictional debonding and slip much easier to occur.

5. Damping mechanism in fine fiber-reinforced concrete

Fine fiber (6 mils in diameter with a smooth surface) used in this study had an aspect ratio of about 170. According to Fig. 4, the debonding can only take place at the ends of an interface. If the debonding could occur only in a very small fraction of the whole interface, the damping would not be discernible. The experimental observations, however, showed the damping in this FRC was better than in plain concrete. Concrete is a brittle material in which micro and potential cracks are pervasive [15]. SEM observations showed that an interface was always surrounded by microcracks [1,4]. An assumption can therefore be made that the interaction between fiber and surrounding cracks would come into effect as the matrix is strained. A distribution of these cracks surrounding an interface is schematically illustrated as in Fig. 6. As the surrounding matrix is strained in tension, the cracks open. The opening of each crack is dependent on the strain and the crack density along the interface. According to fracture mechanics [16], the mode I crack opening is proportional to the tensile stress perpendicular to the crack. It is assumed that the crack opening, δ_c, is proportionally associated with the total elongation of the matrix with an effective length l_{eff}, as indicated in Fig. 6. This may be a reasonable approximation because the interruption of stress flow greatly reduces strain in the matrix between cracks (not including the tips of the crack where stress concentration occurs). Therefore, Eq. (17)

$$\delta_c = k_\delta \varepsilon_m l_{eff} \tag{17}$$

where k_δ is a proportional constant ($0 \le k_\delta \le l$).

A total relative displacement, δ, along the entire interface can be summed up as Eq. (18)

$$\delta = \sum \delta_c = k_\delta \varepsilon_m \sum l_{eff} \tag{18}$$

or

$$\delta = k_\delta \varepsilon_m l \tag{19}$$

where l is the interface length which approximately equals the fiber length.

Substituting data for a 6-mil (0.152 mm) fiber which is 1 in. (25.4 mm) long into Eq. (19), we have $\delta = (2.8–22.4) \times$

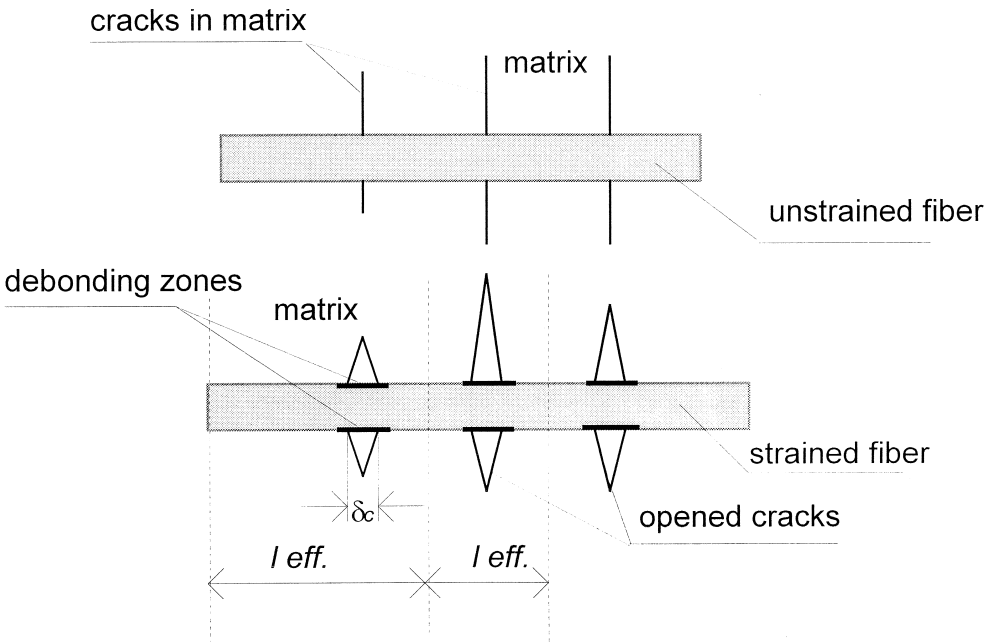

Fig. 6. Illustration of cracks in cementitious matrix surrounding reinforcing fiber and crack openings under tensile strain.

$10^{-8}\,k_\delta$ m, as ε_m varies from 1.1×10^{-6} to 8.8×10^{-6}. This relative displacement, if $k_\delta = 1$, is two orders greater than that calculated from Eq. (10), which yields $\varepsilon_m/\beta = (0.73 - 5.87) \times 10^{-10}$ m. The total relative displacement along a fiber without considering cracks is too small to compare with that considering cracks.

Assuming the interface bond strength is τ_s, and therefore, the bond strength per unit length of an interface equals $\pi d_f(1)\tau_s$. The energy dissipated on the entire interface, W_d, due to debonding and friction caused by crack opening can be estimated by Eq. (20)

$$W_d = \pi d_f(1)\tau\delta = \pi d_f \tau(1) k_\delta \varepsilon_m l. \tag{20}$$

By using the data for 6-mil fiber with a shear strength of 0.5×10^{-2} MPa, as calculated in the previous section, required to initiate an interfacial debonding under a maximum matrix strain of 1.1×10^{-6}, as observed in our experiments, we have $W_d = 6.7 \times 10^{-8}\,k_\delta$ J. The energy dissipated due to crack closing which may, though not necessarily, occur in the compressive part of the beam in the first cycle of vibration is smaller than that due to the opening, because only frictional slip may be involved. The damping caused by such frictional slip may contribute to a part of the damping ratio ζ_{10}, as shown in Fig. 1.

The maximum (uniaxial) strain energy, dU, in an infinitesimal volume, dV, of a beam is given by Eq. (21)

$$dU = \frac{1}{2} E_m \varepsilon_M^2 dV. \tag{21}$$

Substituting Eq. (2) into the above equation yields Eq. (22)

$$dU = \frac{1}{2} E_m \left\{ \frac{A_M y}{2l^2} \left[\frac{d^2 v(x_l)}{dx^2} \right] \right\}^2 dV. \tag{22}$$

The maximum strain energy of the beam, U_{Mstr}, which is equal to the total vibration energy, is therefore given by Eq. (23)

$$U_{Mstr} = 2 \int_0^{h/2} \int_0^{l} \int_0^{b} dU \tag{23}$$

where h, l, and b are the thickness, the length, and the width of the beam, respectively.

Using the data for $(d^2v(x/l))/dx^2$ given by Young and Flegar [8], $E_m = 28$ GPa, $A_M = 10^{-5}$ m, $l = 0.3$ m, $b = 0.1$ m, and $y_{max} = h/2 = 0.0125$ m, we have $U_{Mstr} = 1.69 \times 10^{-6}$ J.

Neglecting the energy dissipation due to the crack closing, a specific damping capacity (ratio of energy dissipated to the total energy input) resulting from crack opening along one such interface is 0.04, which can be converted to an equivalent damping ratio of 0.325% [6]. It can been seen from Fig. 1 that the difference in damping ratio between ζ_1 and ζ_{10} at the maximum response amplitude of 0.001 cm is about 1.0%. This indicates that three or four such interfaces in the surface layer of the beam were involved in the energy dissipation. This estimation seems quite reasonable when compared to the observation of fiber distribution in specimens (low-volume fraction fibers which were randomly distributed).

When a fiber has a coarse diameter, and thus a large circumference, the resistance to crack opening is greater at the same level of matrix strain. The 25-mil smooth surface fiber did not produce an improvement in damping, probably because of its large circumference and surface defibrillation by mixing [1,4], resulting in large resistance to crack opening. The 15-mil smooth surface fiber reinforcement exhibited some improvement in damping at a specimen age of 8 weeks, but no improvement at age of 24 weeks until the maximum response amplitude exceeded 0.008 cm [1,2]. This may be due to an increase in bond strength with the curing time.

It is inferred that the debonding in these FRCs might still take place if the vibration amplitude becomes large enough. On the other hand, if the amplitude is small, damping for all FRCs and plain concrete would not be of much difference until the input energy is sufficient to change the bonding conditions. It is therefore concluded that an increased damping must be triggered by certain threshold energy. The magnitude of this energy would depend on the bonding conditions. As soon as this debonding has taken place, it is possible that a relative movement, or slip, between fiber and matrix takes place along the interface. The matrix would be rubbing on the fiber under an alternating strain; the vibration energy thus being further dissipated through interfacial friction. Therefore, the interfacial friction is the mechanism for vibration cycles after the first cycle. Obviously, the energy dissipated through this slip is not as great as through debonding. The damping of this mechanism may be strain dependent (since the maximum response amplitude varies within a certain range), and repeatable as the same amplitude within this range is reproduced. When the maximum response amplitude exceeds this range due to a heavy impact, an increase in microcrack length and number may result. Additional energy is thus consumed. The damping ratio will not be the same before and after this heavy impact even though the amplitude is within the small range.

6. Conclusions

On the basis of preliminary experiments and theoretical analysis, two damping mechanisms in polyolefin FRC have been suggested. These explain how vibration energy is dissipated through interfacial debonding and friction in the crimped fiber and the fine-FRC, respectively. In the crimped FRC, a great fraction of the low-aspect ratio segmental interface may be subject to a significant relative displacement that causes debonding. In the fine fiber-reinforced composites, debonding, and interfacial friction may take

place at the intersections of fiber and microcracks in the surrounding matrix through crack opening under tensile strain. It is inferred that, in order to gain good damping, fibers with a diameter less than 6 mils should be used. On the other hand, low-aspect ratio fiber, with a diameter greater than 6 mils, is also a prospective candidate for good damping. It is noted that an interface roughness due to the defibrillation of fibers produced during mixing may have a significant impact on damping in FRC.

Acknowledgments

This work was supported in part by the National Science Foundation under Grant No. ORS-9108773 and State of South Dakota Future Fund. Dr. L. Rich and Mr. C.N. MacDonald from 3M are gratefully acknowledged for their support in providing partial funding and fibers. Dr. V. Ramakrishnan at South Dakota School of Mines and Technology is also acknowledged for his providing laboratory and materials for casting specimens.

References

[1] L. Yan, Study of dynamic properties and interfaces of synthetic fiber reinforced cement composites, PhD dissertation, South Dakota School of Mines and Technology, 1996.
[2] L. Yan, R.L. Pendelton, C.H. Jenkins, Polyolefin fiber reinforced concrete composites: Part I. Damping and frequency characteristics, Cem Concr Res 30 (3) (2000) 391–401.
[3] L. Yan, R.L. Pendleton, The dynamic properties of polyolefin fiber reinforced concrete composites, Proc ICCE/3, New Orleans, 1996, pp. 671–672.
[4] L. Yan, R.L. Pendleton, C.H. Jenkins, Interface morphologies in polyolefin fiber reinforced concrete composites, Composites Part A 29A (1998) 643–650.
[5] Z.P. Bazant, Z. Li, M. Thoma, Identification of stress–slip law for bar or fiber pullout by size effect tests, J Eng Mech May (1995) 620–625.
[6] A.A. Shabana, Theory of Vibration, Vol. II, Springer-Verlag, New York, 1991.
[7] R.C. Hibbeler, Mechanics of Materials, 2nd edn., Prentice-Hall, Englewood Cliffs, NJ, 1994, pp. 583–584.
[8] D. Young, R.P. Felgar Jr., Tables of characteristic functions representing normal modes of vibration of a beam, The University of Texas Publication No. 4913, July 1, 1949.
[9] D. Hannant, Fiber Cements and Fiber Concrete, Wiley, New York, 1978, pp. 81–91.
[10] R.G. White, E.M.Y. Abdin, Dynamic properties of aligned short fiber-reinforced plastics in flexure and torsion, Composites 12 (1985) 293–306.
[11] H.L. Cox, The elasticity and strength of paper and other fibrous materials, Br J Appl Phys 3 (1952) 72–79.
[12] A. Kelly, Strong Solids, 2nd edn., Clarendon Press, Oxford, England, 1973.
[13] R.F. Gibson, Principles of Composite Material Mechanics, McGraw-Hill, New York, 1994, pp. 162–164.
[14] Y. Wang, S. Backer, V.C. Li, An experimental study of synthetic fiber reinforced cementitious composites, J Mater Sci 22 (1987) 4281–4291.
[15] S. Diamond, A. Bentur, On the cracking in concrete and fiber reinforced cement, in: S.P. Shah (Ed.), Application of Fracture Mechanics to Cementitious Composites, Martinus Nijhoff Publishers, Dordrecht, 1985, pp. 87–140.
[16] K. Hellan, Introduction to Fracture Mechanics, McGraw-Hill, New York, 1984, pp. 235–242.